2016 12th International Conference on Signal-Image Technology & Internet-Based Systems

Longitudinal Neuroimaging Analysis Using Non-Negative Matrix Factorization

Claudio Stamile
Department of Electrical Engineering (ESAT), STADIUS
Katholieke Universiteit Leuven, Belgium
Email: Claudio.Stamile@esat.kuleuven.be

François Cotton
CREATIS, CNRS UMR5220, INSERM U1044,
Université de Lyon, Université Lyon 1, INSA-Lyon,
Lyon, France
Email: francois.cotton@chu-lyon.fr

Dominique Sappey-Marinier
CREATIS, CNRS UMR5220, INSERM U1044,
Université de Lyon, Université Lyon 1, INSA-Lyon,
Lyon, France
Email: dominique.sappey-marinier@univ-lyon1.fr

Sabine Van Huffel
Department of Electrical Engineering (ESAT), STADIUS
Katholieke Universiteit Leuven, Belgium
Email: Sabine.Vanhuffel@esat.kuleuven.be

***Abstract*—Longitudinal analysis of neuroimaging data is becoming an important research area. In the last few years analysis of longitudinal data become a crucial point to better understand pathological mechanisms of complex brain diseases such as multiple sclerosis (MS) where white matter (WM) fiber bundles are variably altered by inflammatory events.**

In this work, we propose a new fully automated method to detect significant longitudinal changes in diffusivity metrics along WM fiber-bundles. This method consists of two steps: *i)* preprocessing of longitudinal diffusion acquisitions and WM fiber-bundles extraction, *ii)* application of a new hierarchical non negative matrix factorization (hNMF) algorithm to detect "pathological" changes.

This method was applied first, on simulated longitudinal variations, and second, on MS patients longitudinal data. High level of precision, recall and F-Measure were obtained for the detection of small longitudinal changes along the WM fiber-bundles.

***Keywords*-Non-Negative Matrix Factorization, White Matter, Multiple Sclerosis, Tractography, Longitudinal Analysis**

I. Introduction

Longitudinal analysis of neuroimaging data is becoming an important research area. In the last few years analysis of longitudinal data become a crucial point to better understand pathological mechanisms of complex brain diseases such as multiple sclerosis (MS) where white matter (WM) fiber bundles are variably altered by inflammatory events. Since pathological mechanisms remained unknown in certain brain diseases, the investigation of their temporal progression using non-invasive neuroimaging techniques is essential to better understand and predict the disease evolution and manage the therapeutic treatment [17][7]. As the etiology of multiple sclerosis (MS) as well as the pathological mechanisms including inflammatory and neurodegenerative processes, are not well understood, longitudinal studies using advanced MRI techniques such as diffusion tensor imaging (DTI) providing sensitive markers, like fractional anisotropy (FA) and radial diffusivity (λ_r), constitute the best potential for the characterization of brain tissue alterations. For example, the analysis of grey matter (GM) structures [8] showed the capability to evaluate the dynamics disability progression; while in white matter (WM) [11] a relationship between damaging and reparative mechanisms that occur in the lesions formation is underlined. By merging the spatial information of fiber tracking [9] with the diffusion metrics derived from the diffusion tensor, it is possible to characterize the presence of "pathological" events that may occur along afferent WM fiber pathways leading to antero- or retrograde degeneration. Thus, for a better understanding of the spatial and temporal progression of MS pathological processes, an accurate and sensitive characterization of WM fibers along their pathways is needed. As shown in our previous work [13] a global approach to analyze disease evolution was not sensitive enough to detect small and short-term (daily/weekly) longitudinal variations occurring typically in relapsing remitting (RR) MS patients. A local scale approach is thus necessary to detect the presence of small "pathological" changes that could only affect a small subset of the WM fiber-bundle. In [14] we proposed a genetic algorithm method to detect longitudinal variations on FA histogram occurring along WM fiber-bundle in MS patients.

In this work we present a new fully automated method based on non-negative matrix factorization (NMF) using all the DTI derived metrics to detect small longitudinal variations occurring along the WM fiber-bundle in MS patients.

This paper is structured as follows. In Section II, we provide a detailed description of our approach. In Section III, we present our experimental campaign. Finally, in Section IV, we draw our conclusions.

II. Description of the proposed approach

The proposed method is divided in two main parts: *i)* preprocessing of longitudinal diffusion acquisitions and WM fiber-bundles extraction, *ii)* application of a new model to detect "pathological" phenomena occurring along WM fiber bundles.

978-1-5090-5698-9/16 $31.00 © 2016 IEEE
DOI 10.1109/SITIS.2016.18

IEEE computer society

A. Preprocessing and fiber-bundle extraction

As first step, each of the s time-points ($T_1 \dots T_s$) of DTI longitudinal acquisitions, are processed in order to compute six different diffusion maps: FA, MD, radial diffusivity (λ_r) and the three eigenvalues of the diffusion tensor λ_1 (also called axial diffusivity), λ_2, λ_3. All the six maps of each time-point are then co-registered on the respective maps obtained at the first time-point (T_1) using a rigid registration algorithm [4]. Orientation distribution function (ODF) and probabilistic tractography [16] are computed using the information of T_1 acquisition. The result of the tractography is then used to extract and post-process WM fiber-bundles. The extraction is performed using a semi-automatic algorithm [15] coupled with the prior knowledge extracted from the JHU WM fiber-bundle atlas [3]. In order to analyze white matter fiber-bundles an additional step is needed. Indeed the output of the tractography could not be directly used for the analysis of the fiber-bundle since the number of points used to reconstruct the fibers variates. Moreover start and end point of each fiber could not be consistent within the same fiber bundle, fibers could start randomly from the two extremities of the bundle. In order to overcome those problems part of the pipeline described in [13] was applied to process the fiber-bundle. As first step we define common start/end points of each fiber within the bundle. A classical K-Means algorithm [6] is performed to generate two different clusters, R_1 for the starting points and R_2 for the ending points. Fiber points are then reordered from R_1 to R_2 and fibers that did not link the two clusters (broken fibers) are automatically removed. As ulterior step each fiber is resampled with the same number $c = 100$ of points (also called nodes).

After the post-processing we can formalize the extracted fiber-bundle as set $F = \{f_1, f_2, \dots, f_z\}$ composed of z fibers $f_i = \{\boldsymbol{p_1}, \dots, \boldsymbol{p_c}\}$ where $\boldsymbol{p_q} = (x_q, y_q, z_q) \mid 1 \leq q \leq c$. The coordinate $\boldsymbol{p_q}$ is used to extract the voxel's value of one of the six diffusion maps ($FA(\boldsymbol{p_q})$ in case of FA) in the corresponding location of f_i. By fixing the index q in each fiber $f \in F$ it is possible to analyze the global diffusion values in a particular cross-section of F. More in detail, we can collect all the FA values belonging to a given cross-section of F defining the following set: $L_q = \{FA(\boldsymbol{p_q}) \mid \boldsymbol{p_q} \in f \ \forall \ f \in F\}$ where q is the fixed index representing the cross-section to analyze.

B. A NMF based model for longitudinal changes detection

NMF is a blind source separation technique [5], in which a matrix V is approximately factorized into the product of a source matrix W and an abundance matrix H:

$$V \approx W \times H$$

V is a set of non negative data, with m data points on its columns and n features per data point on its rows. The columns of $W \in \mathbb{R}^{n \times k}$ represent the k sources. $H \in \mathbb{R}^{k \times m}$ contains per column the abundance of each of the k sources for one particular data point. In this way, NMF describes each point in a dataset by a linear combination of a predefined number of sources.

In particular, NMF based methods have been shown interesting results in image MRI-based tumor segmentation [12], [10]. NMF aims to extract physically meaningful sources, corresponding to tissue-specific patterns. It is an unsupervised technique, i.e. it can be applied on a patient-by-patient basis without the need for a large training dataset. NMF assesses the relative contribution of each tissue type within each voxel, assuming the dataset can be modeled as a linear combination of the constituent tissue types. The mathematical formulation of the basic NMF problem to perform the factorization is:

$$\begin{aligned} \underset{\boldsymbol{W},\boldsymbol{H}}{\text{minimize}} \quad & f(\boldsymbol{W},\boldsymbol{H}) = \frac{1}{2}\|V - W \times H\|_F^2 \\ \text{subject to} \quad & \forall\ i,j : W_{i,j}, H_{i,j} \geq 0 \end{aligned}$$

In this work, an alternating least-squares algorithm [2] is used to solve the NMF problem.

Let $\boldsymbol{v} \in \mathbb{R}^3$ be a voxel of a given image I. We define as $I(\boldsymbol{v})$ the intensity value of the image I in the voxel $\boldsymbol{v}$. In our longitudinal framework, we define as $I_{p,M}$ the image of the marker M (where M with $|M| = m$ could be one of the six DTI maps) acquired at time-point p. Moreover we denote with $I_{p+a,M}$ the image of the same subject, and with the same marker, acquired $a > 0$ weeks later with respect to the acquisition of $I_{p,M}$.

Since we apply the algorithm in each cross-section separately, we define with D ($|D| = s$) the set of voxels $d \in \mathbb{R}^3$ contained in the specific cross-section of the fiber-bundle to analyze.

Our NMF method is based on a sequential application of the NMF factorization algorithm on two levels of data (V_1 and V_2) as described in figure 2.

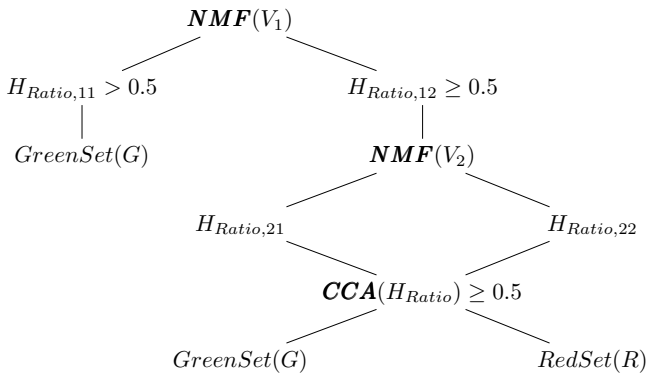


Figure 2. NMF hierarchical longitudinal model

In the first level, the matrix $V_1 \in \mathbb{R}^{2m \times s}$ containing the longitudinal signal information is factorized in $k = 2$ sources using NMF. The matrix is defined as:

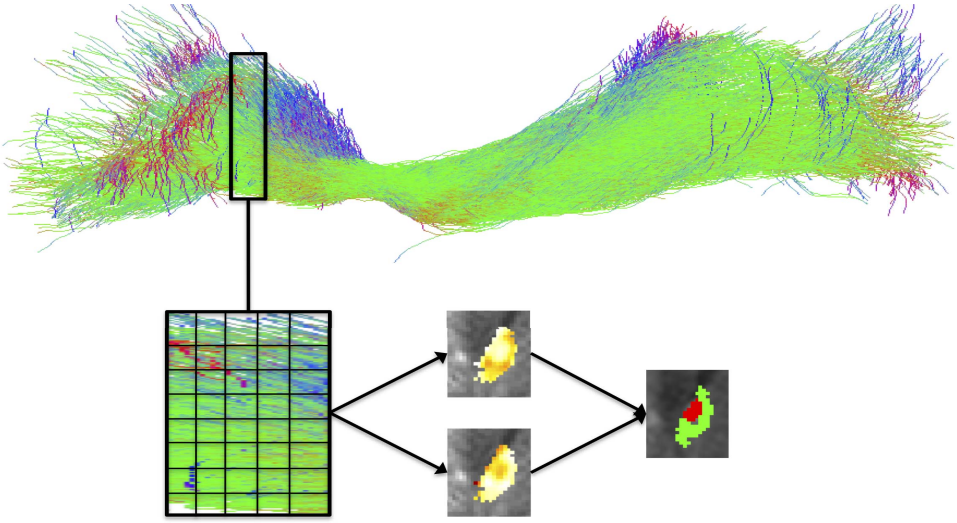


Figure 1. Longitudinal "pathological" variations detected (in red) in a cross-section of the fiber-bundle

$$V_1 = \begin{array}{c} \\ I_{p,M_1} \\ \vdots \\ I_{p,M_m} \\ I_{p+a,M_1} \\ \vdots \\ I_{p+a,M_m} \end{array} \begin{array}{c} \begin{array}{cccc} d_1 & d_2 & \dots & d_s \end{array} \\ \begin{pmatrix} a_{11} & \dots & \dots & a_{1s} \\ \vdots & \vdots & \ddots & \vdots \\ \dots & a_{22} & \dots & a_{2s} \\ \dots & \dots & \dots & \dots \\ \vdots & \vdots & \ddots & \vdots \\ \dots & \dots & \dots & a_{2*ms} \end{pmatrix} \end{array}$$

V_1 contains the feature values of each of the two time-points (I_p and I_{p+a}) for all the voxels $d \in D$ extracted in a given cross section q. Thus, for a voxel d_i belonging to the cross section of the fiber-bundle, its feature vector, containing all the DTI maps, is identified by the $i-th$ column of the matrix V_1.

The application of the first level of our hNMF to V_1 allows to obtain two abundance matrices. We denote with $H_{1,1}$ and $H_{1,2}$ respectively the abundance matrix of the first and second source obtained at the first level of the hNMF model.

The two matrices are then used to compute the H_{Ratio} matrices according to the following formulation:

$$H_{Ratio,ij} = \frac{H_{i,j}}{\sum_{t=1}^{k} H_{i,t}} \qquad (1)$$

voxels having $H_{Ratio,11} > 0.5$ (and thus $H_{Ratio,12} < 0.5$) are marked as voxel not affected by the longitudinal variations and assigned to the *GreenSet* (G). Those voxels belong to the source that generated the signal values of I_{p+a}. Consequently, voxels having $H_{Ratio,12} \geq 0.5$ (and thus $H_{Ratio,11} < 0.5$) are marked as affected by general longitudinal variations. Those voxels belong to a different source than the one that generated values of I_p. This second source could contain: new noise, methodological errors (like registration errors), biological differences or variations generated by the presence of certain pathologies.

In order to check and, eventually, isolate voxels affected by pathological phenomena, the second level of our hNMF model is executed on voxels contained in $T = D - G$ with $|T| = t$. Starting from this subset of voxels, the matrix $V_2 \in \mathbb{R}^{m \times t}$ is obtained from V_1 taking only the features belonging to the $I_{p+q,M_{1,\dots,m}}$ and the voxels $z \in T$.

$$V_2 = \begin{array}{c} \\ I_{p+a,M_1} \\ \vdots \\ I_{p+a,M_m} \end{array} \begin{array}{c} \begin{array}{cccc} z_1 & z_2 & \dots & z_t \end{array} \\ \begin{pmatrix} \dots & a_{12} & \dots & a_{1t} \\ \vdots & \dots & \ddots & \vdots \\ \dots & \dots & \dots & a_{mt} \end{pmatrix} \end{array}$$

As for the first hierarchical level, NMF is applied to V_2 and the matrix is factorized in $k = 2$ sources. We denote with $H_{2,1}$ and $H_{2,2}$ respectively the abundance matrix of the first and second source obtained at the second level of our hNMF model.

Those two matrices are then used to compute the H_{Ratio} matrices using the equation 1. Once H_{Ratio} matrices are computed for the second level, in order to check the presence of "pathological" regions in $H_{Ratio,21}$ or $H_{Ratio,22}$, analysis of connected component regions (CCA) is performed on voxels having $H_{Ratio,21} \geq 0.5 \vee H_{Ratio,22} \geq 0.5$. Connected component regions larger than β voxels and having FA differences, with respect to the reference time point I_p, larger than $\gamma\%$ are marked as "pathological" regions. Voxels belonging to these regions are assigned to the *RedSet* (R) while the other voxels are assigned to G.

III. Experiments

A. Experiment on simulated longitudinal variations

Our algorithm was first tested on a control subject who benefitted from two weekly MR examinations (I_1 and I_2) including a DTI and FLAIR acquisitions, that were performed on a 3T Philips Achieva system (Philips Healthcare, Best, The Netherlands) with a 32-channels head-coil. The DTI protocol consisted of the acquisition of

60 slices of 2 mm thickness oriented in the bi-commissural plan (AC-PC) using a 2D Echo-Planar Imaging (EPI) sequence (TE/TR = 60/800 ms, FOV = 224x224x120 mm) with 32 gradient directions (b = 1000 $s.mm^{-2}$). The nominal voxel size at acquisition (2x2x2 mm) was interpolated to 0.875x0.875x2 mm after reconstruction. The FLAIR Vista 3D sequence (TE/TR/TI = 56/8000/ 2400 ms, FOV=180x250x250 mm) consisted of the acquisition of 576 slices of 0.43 mm thickness oriented in the AC-PC axis with a nominal voxel size of 0.6x0.43x0.43 mm.

120 different lesions were simulated on the control subject's diffusion maps obtained at T_2. All the lesions were generated in 6 different fiber-bundles, namely, left and right, cortico-spinal tract, inferior-fronto occipital fasciculi and forceps major and minor of corpus callosum. Small spherical variations (radius of 3 voxels equals to $2.6mm$ spherical lesions) of diffusion values were generated according to the following equations:

$$\lambda_2^* = \lambda_2 + \alpha * (\lambda_1 - \lambda_2) \quad \lambda_3^* = \lambda_3 + \alpha * (\lambda_1 - \lambda_3)$$

where $0 < \alpha < 1$ is the *reduction coefficient* used to simulate the percentage of longitudinal changes between the two time-points and $\lambda_1, \lambda_2, \lambda_3$ are the three eigenvalues obtained from the DTI. Derived diffusion metrics like FA, MD and λ_r were recomputed according to the new value of λ_2^* and λ_3^*. DTI metrics: FA, MD, λ_r, λ_1, λ_2, λ_3 were used as features for the V_1 matrix. The capability to detect the presence of longitudinal variations between two time-points was tested. Two different tests were run using hNMF. In the first test each NMF of the two levels was randomly initialized using random matrices, while in the second step precomputed initialization was used to initialize each NMF. Detection performances were quantified in terms of Precision, Recall and F-Measure. Moreover we tested the capability of our method to well delineate the regions affected by the longitudinal changes. Sørensen-Dice (DSC) scores were computed according to the following equation:

$$DSC = \frac{2 * |A \cap B|}{|A| + |B|}$$

where A is the voxel set containing the simulated longitudinal variations and B is the voxel set with the longitudinal variations detected by our method. According to this index, we can have three different cases:

1) $DSC = 0$: No overlap
2) $0 < DSC < 1$: Partial overlap
3) $DSC = 1$: Complete overlap

1) Random Initialization: Twenty random non-negative matrices were generated in order to compute the NMF in each of the two levels of our hNMF algorithm. According to the spatial resolution of our images we used as β threshold value 9 voxels while, in order to minimize the presence of false positive given by normal biological variations, we used as $\gamma \geq 0$ threshold value 10% variation. For each NMF in the hNMF model 100 iterations were performed.

Performance values of Precision, Recall and F-Measure are shown in table I. Specificity of the method on this simulated data was 96.7%.

Since we simulated multiple longitudinal changes along the fiber-bundles, we use the mean DSC ($\overline{DSC}$) $\pm$ its standard deviation (σ), to analyze the overlap performance for each α value. Results are also shown in table I.

Table I
EVALUATION (IN %) OF LONGITUDINAL CHANGES DETECTION ON SIMULATED DATA USING RANDOM INITIALIZATIONS.

α	Precision	Recall	F-Measure	$\overline{DSC}$	$\pm\sigma$
0.1	88.9	26.7	41.0	23.8	26.0
0.2	95.1	64.2	77.0	54.3	32.4
0.3	96.6	93.3	95.0	68.6	21.3
0.4	96.5	92.5	94.0	74.5	23.5
0.5	96.4	90.0	93.0	78.6	25.8
0.6	96.6	95.0	96.0	86.4	19.9
0.7	96.5	90.1	94.3	85.5	22.7
0.8	96.5	92.5	94.5	88.7	19.7
0.9	96.5	92.5	94.5	85.9	24.7

2) Smart Initialization: Instead of using multiple random initializations in each level of our hNMF model, the algorithm ALS is run once using as initial W matrix the matrix obtained using the Nonnegative Double Singular Value Decomposition (NNDSVD) method [1]. As for the random initialization the β threshold value was set to 9 voxels and γ threshold value was set to 10% variation. For each NMF in the hNMF model 100 iterations were performed. Performance values of Precision, Recall and F-Measure are shown in table II. Specificity of the method on this simulated data was 80.0%.

Table II
EVALUATION (IN %) OF LONGITUDINAL CHANGES DETECTION ON SIMULATED DATA USING NNDSVD INITIALIZATION.

α	Precision	Recall	F-Measure	$\overline{DSC}$	$\pm\sigma$
0.1	60.0	30.0	40.0	26.8	26.8
0.2	79.1	75.8	77.0	59.6	27.2
0.3	82.9	96.7	89.0	69.0	24.5
0.4	82.4	95.0	88.0	77.0	22.6
0.5	82.4	93.3	88.0	82.1	21.2
0.6	83.2	99.2	90.0	83.7	21.7
0.7	83.0	97.5	90.0	86.2	20.0
0.8	82.7	95.8	89.0	91.0	14.5
0.9	82.2	92.5	87.0	89.8	17.4

Results show that random initialized hNMF outperforms NNDSVD initialized hNMF. More in detail, the random initialized hNMF shows high values in terms of Precision and F-Measure compared to NNDSVD initialized hNMF. Furthermore, no significant differences (according to the Wilcoxon signed-rank test) in terms of DSC were found between the random initialized and the NNDSVD initialized version of our hNMF algorithm.

3) Algorithms Comparison: The capability to detect the presence of longitudinal variations using random initialized hNMF (RhNMF) and the smart initialized hNMF (ShNMF) were compared to our previous method described in [14] (GA). Precision Recall and F-Measure of the three methods were compared on the same simulated

dataset. Comparison of the performances measure are displayed in table III

Table III
PERFORMANCES COMPARISON OF THE CAPABILITY TO DETECT LONGITUDINAL CHANGES BETWEEN: STAMILE ET. AL 2015 [14] (GA), RANDOM INITIALIZED HNMF (RHNMF) AND SMART INITIALIZED HNMF (SHNMF)

	Precision			Recall			F-Measure		
α	GA	RhNMF	ShNMF	GA	RhNMF	ShNMF	GA	RhNMF	ShNMF
0.1	62.8	88.9	60.0	45.0	26.7	30.0	52.4	41.0	40.0
0.2	73.1	95.1	79.1	72.5	64.2	75.8	72.8	77.0	77.0
0.3	77.1	96.6	82.9	90.0	93.3	96.7	83.1	95.0	89.0
0.4	77.1	96.5	82.4	90.0	92.5	95.0	83.1	94.0	88.0
0.5	77.3	96.4	82.4	90.1	90.0	93.3	83.5	93.0	88.0
0.6	77.6	96.6	83.2	92.5	95.0	99.2	84.4	96.0	90.0
0.7	77.9	96.5	83.0	94.1	90.1	97.5	85.5	94.3	90.0
0.8	77.9	96.5	82.7	94.1	92.5	95.8	85.5	94.5	89.0
0.9	77.9	96.5	82.2	94.1	92.5	92.5	85.5	94.5	87.0

The average Precision for GA, RhNMF and ShNMF was respectively 75.4%, 95.4%, 79.4%, the average Recall was 84.7%, 81.9%, 86.2% and the average F-Measure was 79.5%, 86.6%, 82.0%. Overall, RhNMF shows better performances in terms of Precision and F-Measure compared to GA and ShNMF. GA and ShNMF show just a better average Recall compared to RhNMF respectively: 2.8% and 4.3% better. A detailed analysis shows, as expected, a better capability of GA to distinguish between artifact and pathological phenomena in case of really small longitudinal changes ($\alpha = 0.1$).

We also tested the averaged execution time of the three algorithms. The average execution time for each cross-section for GA, RhNMF and ShNMF is respectively $19.2s$, $1.2s$ and $1.2s$.

B. Application on MS follow-up

Two RR MS patients were included in this study. The patients had to be untreated for at least one year and had at least one active gadolinium enhancing lesion during the six months preceding study enrollment. This study was approved by the local ethics committee ("CPP Sud-Est IV") and the French national agency for medicine and health products safety (ANSM). Written informed consents were obtained from all patients and control subjects prior to study initiation. All patients underwent a weekly DTI examination for a period of two months that was performed using the same acquisition parameters described for the control subject in section III-A. DTI data of each patient were processed using our proposed pipeline described in section II. Among the 20 fiber-bundles extracted in each patient, the Cortico-Spinal Tract (CST) and the Inferior Fronto-Occipital Fasciculi (IFOF) were selected, due to the presence of longitudinal "pathological" alterations.

In order to detect longitudinal variations in a real MS data, random initialization hNMF was used and the thresholds β and γ were respectively set at 9 voxels and 10%.

Results of application of the proposed method on real data are illustrated in Figure 3 and 4. In the figures, both small and large "pathological" longitudinal variations occurring along the two WM fiber-bundles were correctly identified using multiple diffusion features.

IV. CONCLUSION

We described a new fully automated tool for analyzing longitudinal changes in the WM fiber-bundles of MS patients. Particularly, we developed a new model to detect local scale longitudinal variations caused by rapid inflammatory processes in RR patients. NMF was used to detect the presence of "pathological" regions generated during the longitudinal follow-up. Results showed high performances to detect small longitudinal changes in both simulated and real data.

Main advantage of our method is related to the robustness of NMF and to its capability to minimize the effect different longitudinal biases like noise and registration errors take advantage of the multimodal information included in the model. Moreover compared to our previous model [14] we show that RhNMF and ShNMF allow to better detect longitudinal changes. Using RhNMF and ShNMF the computation time, that is usually one of the big problems of GA optimization, decreases drastically. Moreover compared to GA our new NMF based method allows the use of multiple features; indeed the method is faster and includes multiple features. In the future, we plan to improve our method including more MRI modalities (MRS, T2, T1, etc.).

Such improved biomarker identification provides a sensitive approach to better understand pathological alterations occurring during MS disease evolution, if longitudinal data are available.

ACKNOWLEDGMENTS

This work is funded by the following projects: Flemish Government FWO project G.0869.12N (Tumor imaging); Belgian Federal Science Policy Office: IUAP P7/19/ (DYSCO, "Dynamical systems, control and optimization", 2012-2017); Henri Benedictus Fellowship of the Belgian American Educational Foundation. French National Research Agency (ANR) within the national program "Investissements d'Avenir" through the OFSEP project (ANR-10-COHO-002). EU: The research leading to these results has received funding from the European Research Council under the European Union's Seventh Framework Programme (FP7/2007-2013) / ERC Advanced Grant: BIOTENSORS (n 339804). EU MC ITN TRANSACT 2012 (n 316679). This paper reflects only the authors' views and the Union is not liable for any use that may be made of the contained information.

REFERENCES

[1] C. Boutsidis, E. Gallopoulos, "SVD based initialization: A head start for nonnegative matrix factorization," Pattern Recogn., vol. 41(4), pp. 1350-1362, 2008.

[2] N. Gillis, F. Glineur, "Accelerated multiplicative updates and hierarchical ALS algorithms for nonnegative matrix factorization," Neural Comput, vol. 24, pp. 1085-1105, 2012.

[3] K. Hua, J. Zhang, S. Wakana, H. Jiang, X. Li, D. S. Reich, "Tract probability maps in stereotaxic spaces: analyses of white matter anatomy and tract-specific quantification," Neuroimage, vol. 39, pp. 336-347, 2008.

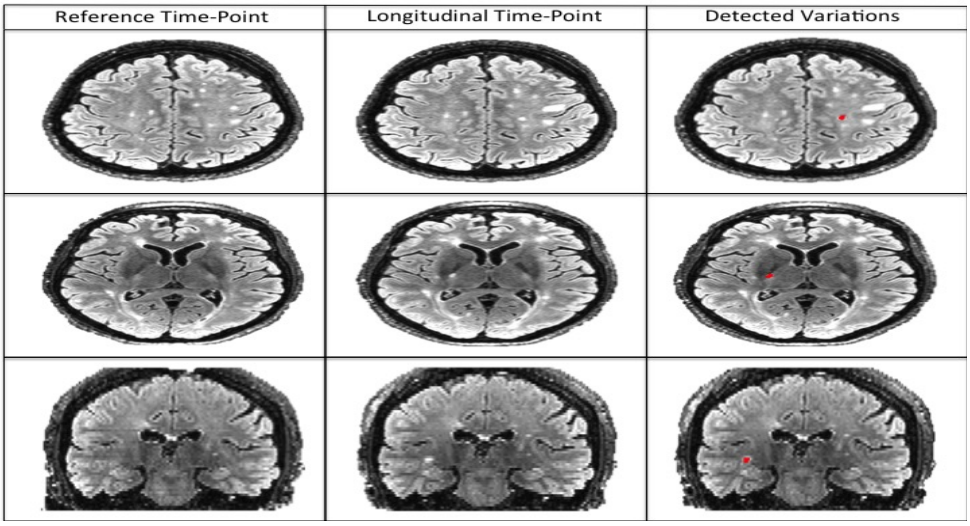


Figure 3. Longitudinal "pathological" variations detected (in red) by the application of our method on left and right CST and right IFOF of two MS patients. The results are superimposed to FLAIR images to better show the lesion.

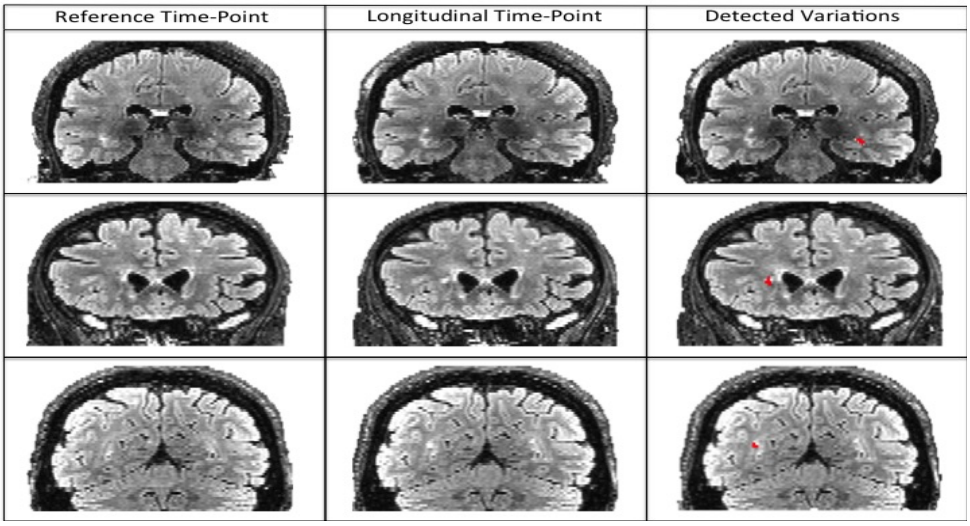


Figure 4. Longitudinal "pathological" variations detected (in red) by the application of our method on right IFOF of two MS patients. The results are superimposed to FLAIR images to better show the lesion.

[4] M. Jenkinson, S. Smith, "A global optimisation method for robust affine registration of brain images," Med Image Anal, vol. 5, pp. 143-156, 2001.

[5] D. D. Lee, H. S. Seung, "Learning the parts of objects by non-negative matrix factorization,", Nature, vol. 401, pp. 788-791, 1999.

[6] J. MacQueen, "Some methods for classification and analysis of multivariate observations," Proceedings of the fifth Berkeley symposium on mathematical statistics and probability, vol. 1(14), 1967.

[7] E. Mak, L. Su, G. B. Williams, J. T. O'Brien, "Neuroimaging correlates of cognitive impairment and dementia in Parkinson's disease," Parkinsonism & Related Disorders, vol. 21(8), pp. 862-870, 2015.

[8] S. Mesaros, M. A. Rocca, E. Pagani, M. P. Sormani, M. Petrolini, G. Comi, M. Filippi, "Thalamic damage predicts the evolution of primary-progressive multiple sclerosis at 5 years," AJNR Am J Neuroradiol, vol. 32(6), pp. 1016-1020, 2011.

[9] S. Mori, B. J. Crain, V. P. Chacko, P. C. van Zijl, "Three-dimensional tracking of axonal projections in the brain by magnetic resonance imaging," Ann Neurol, vol. 45, pp. 265-269, 1999.

[10] S. Ortega-Martorell, P. J. G. Lisboa, A. Vellido, R. V. Simões, M. Pumarola, M. Julià-Sapé, C. Arús, "Convex non-negative matrix factorization for brain tumor delimitation from MRSI data," PLoS ONE 7(10): e47824, 2012.

[11] A. Rovira, C. Auger, J. Alonso, "Magnetic resonance monitoring of lesion evolution in multiple sclerosis," Ther Adv Neurol Disord, vol. 6(5), pp. 298-310, 2013.

[12] P. Sajda, S. Du, T. R. Brown, R. Stoyanova, D. C. Shungu, X. Mao, L. C. Parra, "Nonnegative matrix factorization for rapid recovery of constituent spectra in magnetic resonance

chemical shift imaging of the brain," IEEE Trans. Med. Imaging, vol. 23, pp. 1453-1465, 2004.

[13] C. Stamile, G. Kocevar, F. Cotton, F. Durand-Dubief, S. Hannoun, C. Frindel, D. Rousseau, D. Sappey-Marinier, "A Sensitive and Automatic White Matter Fiber Tracts Model for Longitudinal Analysis of Diffusion Tensor Images in Multiple Sclerosis," PLoS ONE 11(5): e0156405. doi:10.1371/journal.pone.0156405, 2016.

[14] C. Stamile, G. Kocevar, F. Cotton, F. Durand-Dubief, S. Hannoun, C. Frindel, D. Rousseau, D. Sappey-Marinier, "A Longitudinal Model for Variations Detection in White Matter Fiber-Bundles," In Proceeding IWSSIP 2015, pp. 57-60, 2015.

[15] C. Stamile, F. Cauteruccio, G. Terracina, D. Ursino, G. Kocevar, D. Sappey-Marinier, "A Model-Guided String-Based Approach to White Matter Fiber-Bundles Extraction," LNCS 9250, pp. 135-144, 2015.

[16] J. D. Tournier, F. Calamante, A. Connelly, "MRtrix: Diffusion tractography in crossing fiber regions," International Journal of Imaging Systems and Technology, vol. 22, pp. 53-66, 2012.

[17] M. Vandermosten, J. Vanderauwera, C. Theys, A. De Vos, S. Vanvooren, S. Sunaert, J. Wouters, P. Ghesquiére, "A DTI tractography study in pre-readers at risk for dyslexia," Developmental Cognitive Neuroscience, vol. 14, pp. 8-15, 2015.